Applied Catalysis B: Environmental 172–173 (2015) 1–6

Contents lists available at ScienceDirect

Applied Catalysis B: Environmental

journal homepage: www.elsevier.com/locate/apcatb

Highly efficient hydrogen production and formaldehyde degradation by Cu_2O microcrystals

Hong Gao [a], Junying Zhang [a,*], Rongming Wang [b], Mei Wang [a]

[a] Key Laboratory of Micro-nano Measurement, Manipulation and Physics (Ministry of Education), Department of Physics, Beihang University, Beijing 100191, China

[b] School of Mathematics and Physics, University of Science and Technology, Beijing, Beijing 100083, China

ARTICLE INFO

Article history:
Received 17 December 2014
Received in revised form 3 February 2015
Accepted 9 February 2015
Available online 11 February 2015

Keywords:
Cu_2O microcrystal
Hydrogen
Formaldehyde degradation
$[Cu^+]$• paramagnetic
Hydroxyl radical

ABSTRACT

Herein, Cu_2O microcrystals are found to perform efficiently in hydrogen generation and formaldehyde degradation at room temperature, with MgO as a sacrificial agent, while other photocatalytic semiconductors such as TiO_2, ZnO, Bi_2O_3, Fe_2O_3 and CuO exhibit poor capability under the same condition. This peculiarity of Cu_2O microcrystals is comprehensively analyzed, focusing on exploring the formation of $[Cu^+]$· paramagnetic during the reaction, which is first proposed as a principal factor for the hydrogen generation and formaldehyde degradation. Even more exciting, abundant hydroxyl radicals produced during this reaction process are detected via electron paramagnetic resonance spectrometry, which are particularly efficient in oxidizing formaldehyde and producing hydrogen.

1. Introduction

Cuprous oxide (Cu_2O) is an attractive *p*-type oxide semiconductor for solar energy conversion due to its band gap of 2.17 eV, which absorbs visible light, e.g., as a photocatalyst for electrochemical splitting of water and degradation of organic materials [1–5]. As a low cost material, Cu_2O shows low toxicity and good environmental acceptability [6,7]. Until now, extensive research on Cu_2O has focused on morphology control [8–10] and compositing with graphene oxide, C_3N_4, noble metal, TiO_2, WO_3, MoS_2, etc. [11–21]. In fact, the development of new performance for Cu_2O is an ongoing challenge. Exploring new intrinsic performances of Cu_2O microcrystals has been of interest and importance [22–24]. Here a novel property of Cu_2O microcrystals is discovered. It is used in generating hydrogen by degrading formaldehyde solution at room temperature. As far as we know, there have been some reports on the use of metal nanoparticles such as Cu, Au, Pt, Ni, Ag, and Pd to accelerate the rate of hydrogen production from formaldehyde solution [25–31], but these reactions only occur in an alkaline environment.

In this paper, we demonstrate that Cu_2O microcrystals serve as a highly efficient and convenient photo-activator for hydrogen generation from formaldehyde solution under non-alkaline conditions. By optimizing the reaction parameters such as sacrificial agent and crystal morphology, the rate of hydrogen generation is further increased. Photocatalytic activity of Cu_2O {1 1 0} and {1 1 1} facets for decomposition of dye solution was different due to the different atom arrangement [32–35]. Herein, studies of their photochemical activities clearly reveal that lightly truncated rhombic dodecahedra with {1 1 0} surface exhibit superior photochemical properties in comparison with hexapod exposing {1 1 1} surface for the generation of hydrogen in degrading formaldehyde solution. This peculiarity of Cu_2O microcrystals is attributed to their ability to produce photo-generated electrons, hydroxyl radicals and $[Cu^+]$·paramagnetic during the reaction, all of which contribute greatly to the hydrogen evolution. To the best of our knowledge, $[Cu^+]$·paramagnetic has never been used to directly induce the generation of hydrogen, degradation of formaldehyde solution, and production of abundant hydroxyl radicals.

2. Experimental

2.1. Reagents and materials.

Copper nitrate trihydrate [$Cu(NO_3)_2{\cdot}3H_2O$, 99.5%, Tianjin JinKe Fine Chemical Industry Research Institute], formic acid (HCOOH, ≥88%, XiLong Chemical), ammonia solution ($NH_3{\cdot}H_2O$, 25–28%, XiLong Chemical) and formalin (HCHO, 37–40%, XiLong Chemical) were all analytical grade (AR) and used as received without further purification. Powdered TiO_2 (P25, Degussa), MgO (98%,

* Corresponding author. Tel.: +86 10 82315351; fax: +86 10 82315351.
E-mail address: zjy@buaa.edu.cn (H. Gao).

http://dx.doi.org/10.1016/j.apcatb.2015.02.004
0926-3373/

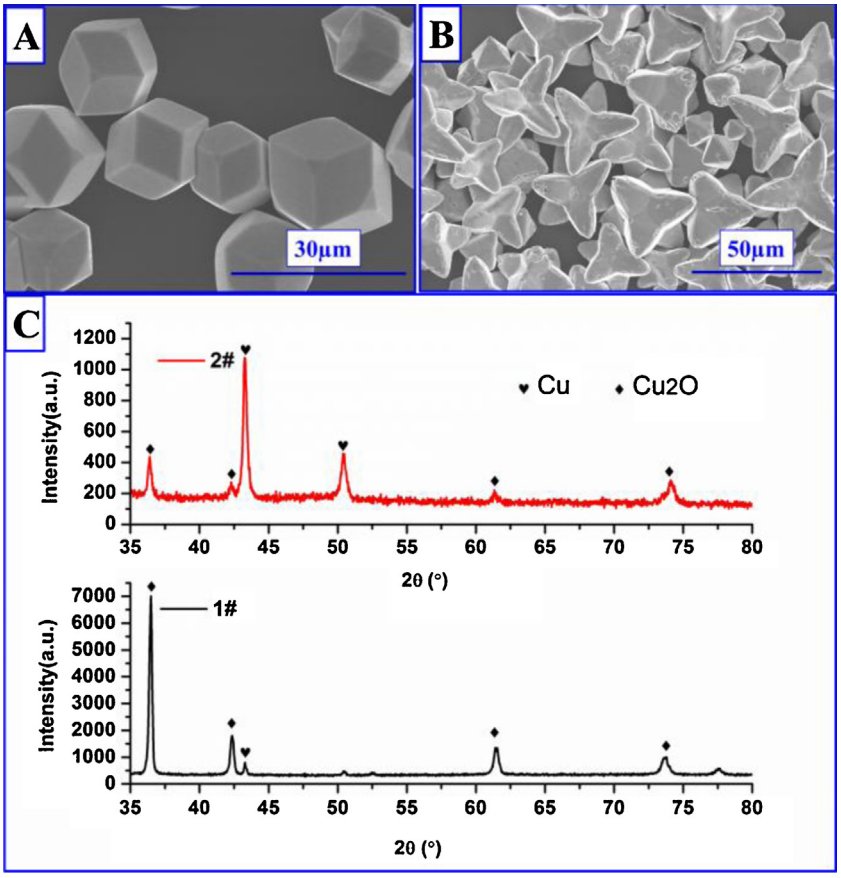

Fig. 1. FE-SEM images of Cu_2O microcrystals with different morphologies: (A) lightly truncated rhombic dodecahedra and (B) hexapod. The XRD patterns of Cu_2O lightly truncated rhombic dodecahedra microcrystals, before (C1#) and after (C2#) their use in generating H_2 through degrading the formaldehyde solution.

Xilong Chemical), ZnO (99.99%, Tianjin JinKe Fine Chemical Industry Research Institute), and CaO (98%, Yili Fine Chemical) were used as received. Absolute ethyl alcohol (C_2H_5OH, 99.7%, AR, Beijing Chemical Works) and deionized water (H_2O, 18 MΩ) were used for all solution preparations and sample washing. The spin trap 5,5-dimethyl-1-pyrrolyne *N*-oxide (DMPO, Dojindo) was analytical grade and diluted to 1 mol/L. Research-grade argon gas (Ar, $V/V \geq 99.9993\%$) and nitrogen (N_2, $V/V \geq 99.9993\%$) were used.

2.2. Cu_2O microcrystal synthesis

$Cu(NO_3)_2{\cdot}3H_2O$ (0.01 mol) was dissolved in mixture solution of H_2O (13 mL) and C_2H_5OH (23 mL) to obtain a blue solution. Then HCOOH (2 mL) and $NH_3{\cdot}H_2O$ were added to the blue solution in sequence. $NH_3{\cdot}H_2O$ was used as a vital agent to tailor the final morphology of the Cu_2O microcrystals [35]. Then, the solutions were transferred into Teflon-lined stainless steel autoclaves, which were all filled to 80% capacity (50 mL) and then supersonically vibrated for 5 min. Afterward, the autoclaves were sealed and heated at 150 °C for 120 min in an oven and then cooled to room temperature naturally. The precipitates were collected and washed with distilled water and ethanol three times, and then dried in the air at room temperature for storage and analysis. Lightly truncated rhombic dodecahedra and hexapod Cu_2O microcrystals were obtained when 3 mL and 1.5 mL of $NH_3{\cdot}H_2O$ were used, respectively.

2.3. Activity tests

The photochemical activities of Cu_2O microcrystals and other photocatalysts were determined by measuring the volume of hydrogen produced from the formaldehyde solution. 10 mg photoactivators and 10 mg sacrifice agents were added into HCHO aqueous solutions [10 mL formalin and 10 mL H_2O] to form mixed solutions, which were put in 50 mL quartz tubes irradiated by a xenon lamp with light intensity about 50 mW/cm^2. Ultraviolet–visible (UV–vis) light was from a xenon lamp and visible light was achieved by a cutoff filter (≥420 nm). Prior to light irradiation, solutions were aerated with Ar for 10 min to remove the air. The quartz tubes were kept at room temperature by circulating water, and the solution was stirred vigorously during the reaction. The evolved gases were analyzed by a gas chromatograph (GC) equipped with a thermal conductivity detector (TCD) and with argon as the carrier gas. No CO or other gaseous product was detected in these processes. A manual head space sampling method is adopted. The needle of gas syringe is used to pierce through the resilient rubber connector for quartz tube and collect 1 mL gas-phase products from the quartz tube. The gas is injected rapidly into GC injector. The percentage of hydrogen is analyzed by GC, and the hydrogen amount can be calculated.

2.4. Instrumentation

The morphologies of the samples were investigated using a field-emission scanning electron microscope (FE-SEM, S-4800Hitachi) operated at an accelerating voltage of 10 kV. The X-ray diffraction (XRD) spectra measurements were performed on a Panalytical X'Pert Pro MPD instrument using Cu Kα radiation (50 kV).

Electron paramagnetic resonance (EPR) spectra were obtained on a JEOL JES-FA200 spectrometer equipped with a liquid nitrogen cryostat. EPR spectra of photo-generated charges were recorded at cryogenic temperatures about 77 K, while measurements using

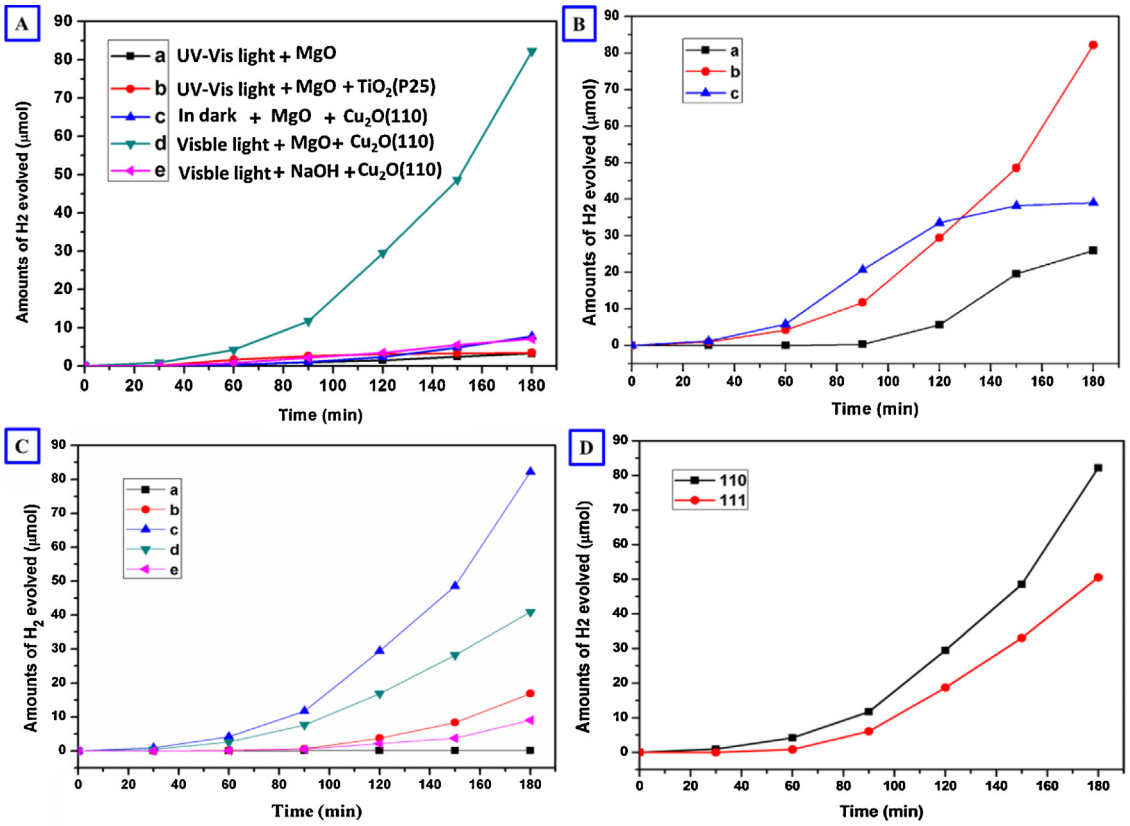

Fig. 2. Time courses of H_2 evolution from HCHO solution. (A) using Cu_2O or TiO_2 as photo-activator and MgO as a sacrificial agent under visible or UV–vis light irradiation. For comparison, control tests in the dark, without photo-activator or using NaOH as sacrificial agent are also presented; (B) by Cu_2O (with{1 1 0} facet) with different sacrificial agents: (a) CaO, (b) MgO, and (c) ZnO; (C) by Cu_2O (with{1 1 0} facet) with different qualities of MgO: (a) 0, (b) 6, (c) 10, (d) 20, and (e) 30 mg; (D) by Cu_2O microcrystals with the {1 1 0} surface (a) and the {1 1 1} surface (b).

DMPO spin trap were performed at room temperature. The test condition for EPR spectrum is that 10 mg MgO, 20 mL HCHO aqueous solutions mixed with 10 mg Cu_2O lightly truncated rhombic dodecahedra under visible light or 10 mg TiO_2 under UV–vis light at room temperature. All solutions were degassed with nitrogen before illumination.

Negative ions in the solutions were measured by ion chromatography (Metrohm 883 Basic IC plus) in the manner of suppression conductivity detection.

3. Results and discussion

FE-SEM images of Cu_2O microcrystals with different morphologies are shown in Fig. 1(A) and (B). Hexapod exposes {1 1 1} facets, while lightly truncated rhombic dodecahedron mainly exposes {1 1 0} facets [35]. Cu_2O and TiO_2 were used as photo-activators to decompose HCHO aqueous solutions under visible or UV–visible lights employing MgO as a sacrificial agent. As shown in Fig. 2(A), Cu_2O microcrystals enclosed with {1 1 0} facets perform well in producing hydrogen from formaldehyde solution. The amount of hydrogen evolution from the formaldehyde solution by TiO_2 is negligible. Likewise, other photo-activator semiconductors, such as ZnO, Bi_2O_3, Fe_2O_3, and CuO, show no activity in producing hydrogen. The effect of OH^- ions on hydrogen evolution is evaluated, as shown in Fig. 2(A-e). The amount of hydrogen evolution is negligible when NaOH is added to the solution to increase the pH value, because the OH^- ion induced hydrogen generation process is temperature dependent [36]. Therefore, it can be inferred that the hydrogen production is greatly dependent on the presence of Cu_2O microcrystals and MgO. In addition, the hydrogen yield by Cu_2O microcrystals under visible light is significantly higher than that in the dark. To sum up, the presence of Cu_2O, MgO, and light illumination are essential to efficiently produce hydrogen from formaldehyde solution as confirmed by Fig. 2(A).

We examined the Cu_2O microcrystals by X-ray diffraction (XRD) before and after their use in hydrogen evolution from formaldehyde solution. As Fig. 1(C) shows, there is a transformation from Cu_2O (JCPDS 78-2076) to Cu (JCPDS 85-1326) in the hydrogen evolution process. We performed two controls: one was that the Cu_2O was replaced by Cu and hydrogen releasing rate was very low, another was that the light was turned off at the second hour during the experiment and the rate of H_2 evolution was declined obviously during the additional four hours. This will be explained in detail below.

Other alkaline oxides instead of MgO were investigated as sacrificial agents in the same experiment condition, as shown in Fig. 2(B). The hydrogen yields by Cu_2O dodecahedra are higher when using MgO as a sacrificial agent than when CaO or ZnO is used. Then, the effect of MgO amount on hydrogen generation was studied, as Fig. 2(C) shows. As the amount of MgO increased from 0 to 10 mg, the hydrogen production rate greatly increased. However, with further increasing the amount of MgO up to 30 mg, the rate of hydrogen production decreased obviously. So the species and amount of sacrificial agents play a key role in this reaction process. The H_2 generation rates (in Fig. 2) were gradually increased as the reaction time prolonged. Usually, there is an induction period in the early stages of the reaction [37–41]. Photo-activators need time to contact with the reaction solution and take light energy. The surface active radical gradually generated on photo-activators and the activity was enhanced. The reaction process is monitored by EPR

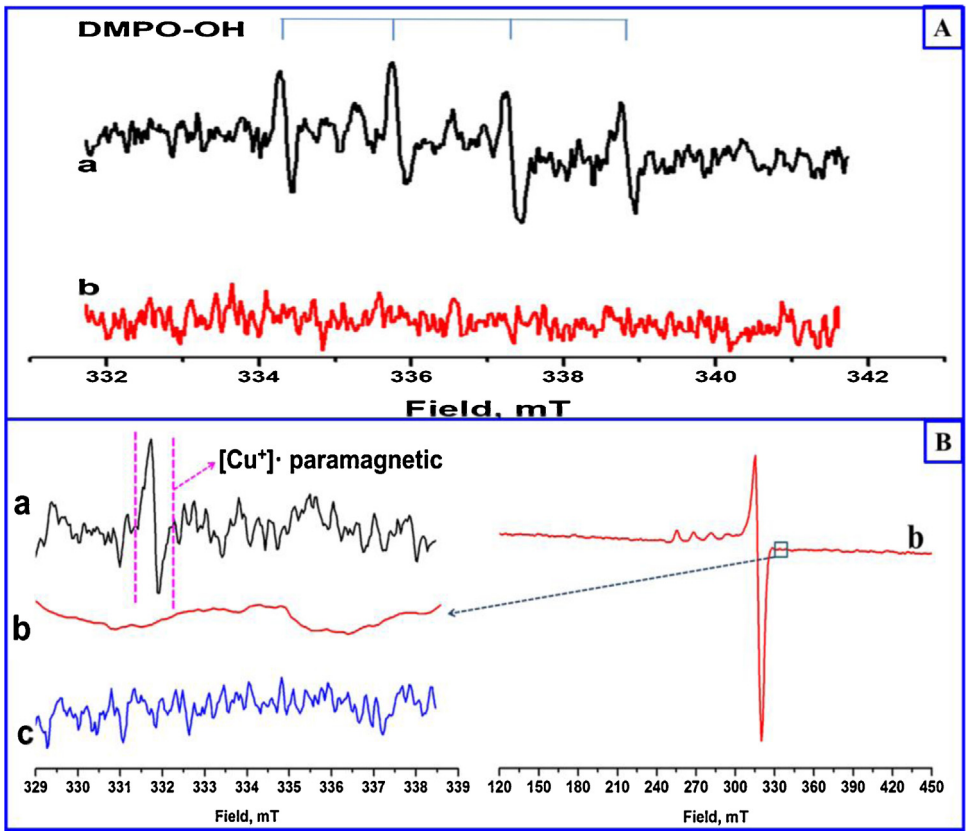

Fig. 3. EPR spectra of solutions containing (A) Cu_2O under visible light (a) or TiO_2 catalyst under UV–vis light (b) at room temperature; (B) Cu_2O (a), Cu_2O without MgO (b), Cu_2O without MgO and HCHO (c), under visible illumination at 77 K.

spectrometer. Cu_2O microcrystals exposing {1 1 0} facets and TiO_2 (P25) were chosen as a catalyst, respectively. MgO was added as a sacrificial agent and DMPO as a spin trap. Signals about the formation of DMPO-OH adducts are observed as shown in Fig. 3(A-a), which does not arise in Fig. 3(A-b). This proves that the formation of hydroxyl radicals is attributed to the presence of Cu_2O.

To elucidate the activity of Cu_2O microcrystals for hydrogen production, EPR measurements were taken at 77 K in order to reduce the charge recombination rate [42]. Fig. 3(B) presents the EPR spectra of different solutions containing Cu_2O lightly truncated rhombic dodecahedra under visible light illumination. A distinct signal at $g_{average} = 1.976$ is shown in Fig. 3(B-a), which approximates to the free electron g-value (2.0023) [43]. The EPR signals with $g_{average} = 1.975$ had been attributed to electrons trapped in the rutile $(Ti^{3+})_{latt}$ [44,45], herein, we associated the EPR signal at $g_{average} = 1.976$ with electrons trapped in Cu^+ lattice, labeled as $[Cu^+]\cdot$paramagnetic. Fig. 3(B-b) shows an observable signature of Cu^{2+} hyperfine lines [46,47] but no signal at $g_{average} = 1.976$. Whereas in Fig. 3(B-c), there is neither observable signature at $g_{average} = 1.976$ nor Cu^{2+} hyperfine lines. In summary, the EPR spectra reveal that the corrosion of Cu_2O and the subsequent Cu^{2+} ion formation in formaldehyde solution occur in the absence of MgO under visible light irradiation, while the presence of both HCHO and MgO contributes to the formation of paramagnetic $[Cu^+]\cdot$.

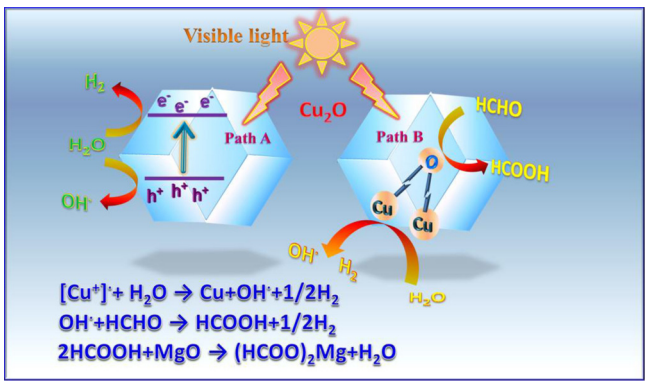

Fig. 4. Schematic of H_2 generation and HCHO degradation process using Cu_2O microcrystals.

Fig. 2(D) reveals that the activity of Cu_2O microcrystals in hydrogen production is closely related to their crystal shapes. When the reaction time reaches 3 h, the amount of hydrogen produced by Cu_2O exposing {1 1 0} surface is 82.2 μmol, while 50.5 μmol hydrogen is produced by Cu_2O exposing {1 1 1} surface. This indicates that {1 1 0} surface of Cu_2O microcrystals shows higher photochemical activity than {1 1 1} surface for the generation of hydrogen from the formaldehyde solution. The amount of $HCOO^-$ ions in the solutions is measured by ion chromatography. There are 21.2 μmol $HCOO^-$ ions in the initial formaldehyde solution, while the amount reaches 774.9 μmol after the reaction. Cannizzaro disproportionation can result in a little existence of $HCOO^-$ ions in formaldehyde solution [25]. Furthermore, the amount of $HCOO^-$ ions has close relationship with Cu_2O morphology. If Cu_2O microcrystals exposing {1 1 1} facets are used, the amount of $HCOO^-$ ions in the formaldehyde solution is 659.9 μmol after the reaction, less than that when Cu_2O microcrystals exposing {1 1 0} facets are used.

Summarizing the above results, we confirm that Cu_2O microcrystal acts as an effective activator and MgO acts as an appropriate sacrificial agent in the process of hydrogen production from formaldehyde solution. Based on the above experimental results, we propose the reaction mechanism depicted in Fig. 4, comprising two paths for the degradation of formaldehyde solution to

hydrogen evolution operated by Cu_2O microcrystals under visible light irradiation. In path A, Cu_2O microcrystals generate electrons (e^-) and holes (h^+) under visible light irradiation, as the literatures reported [1,2]. The photogenerated holes react with H_2O to create hydroxyl radicals and electrons combine with H^+ ions derived from ionization of H_2O to release hydrogen [45,48]. When NaOH is used as a sacrificial agent, H^+ ions are consumed. Hence hydrogen evolution is restrained as shown in Fig. 2(A-e). In path B, the strong reducing HCHO first captures the oxygen atoms from the Cu_2O microcrystal surface under visible light irradiation, and subsequently yields HCOOH. Since the Cu_2O lattice consists of chains of linear —O—Cu^I—O— bonds [3], the Cu^I—O bond of Cu_2O the microcrystal surface is fractured. Cu□Cu forms on the Cu_2O surface, which is the formation of [Cu^+]·paramagnetic confirmed by the peculiar EPR signal at $g_{average} = 1.976$ [Fig. 3(B-a)]. One Cu□Cu indicates an oxygen vacancy between two Cu atoms. The [Cu^+]·paramagnetic possesses a remarkable redox ability in reacting with H_2O to produce hydroxyl radicals along with the evolution of hydrogen as the following equation.

$$[Cu^+]^\bullet + H_2O \rightarrow Cu + OH^\bullet + 1/2H_2 \quad (1)$$

The hydroxyl radicals from both path A and B play an important role in degradation of formaldehyde according to the following reaction:

$$OH^\bullet + HCHO \rightarrow HCOOH + 1/2H_2 \quad (2)$$

The continuous generation of HCOOH raises H^+ ions concentration and results in corrosion of the Cu_2O microcrystal surface. Consequently, all catalytic processes depicted above are blocked, and Cu^+ ions are produced. Furthermore, a dismutation reaction of Cu^+ to Cu metal and Cu^{2+} ions occurs [49]. At this point, only the signature of Cu^{2+} hyperfine lines appears in Fig. 3(B-b), indicating that the generation of [Cu^+]·paramagnetic is inhibited in the absence of MgO. [Cu^+]·paramagnetic directly promotes the generation of hydroxyl radicals and hydrogen. Hence hydrogen quantity decreases substantially in the absence of MgO, as shown in Fig. 2(C). So, HCOOH is desired to be consumed to maintain the appropriate concentration of H^+ and guard against erosion of Cu_2O microcrystals. This is why MgO is added as a sacrificial agent in the solution. Therefore, the phenomena shown in Fig. 2(B) and (C) can be explained. Other sacrificial agents, such as CaO and ZnO, can also consume HCOOH, but MgO performs best. We inferred that CaO can easily react with water and generate $Ca(OH)_2{\cdot}Ca(OH)_2$ can consume HCOOH, but this will change the acid–base degree of reaction process and $Ca(OH)_2$ impedes the Cu_2O microcrystals from fully exploiting light [54]. ZnO possesses amphoteric nature and Zn^{2+} species, such as, $Zn(OH)(HCOO){\cdot}nH_2O$, $Zn(OH)_3^-$ and $Zn(OH)_4^{2-}$, can exist in the solution [50–53]. As a result, HCOOH cannot be consumed. So CaO and ZnO cannot effectively safeguard the solution environment comparing with MgO. Insufficient MgO may be unable to play an effective role in maintaining appropriate concentration of H^+ ions and excessive MgO may impede Cu_2O microcrystals from fully exploiting light, because the reaction rate is mainly limited by the number of catalytic centers [54–57]. When MgO is consumed completely in the experiment, Cu_2O microcrystals begin to translate to Cu. Thus, Cu_2O translates into Cu metal at the end of the experiment, as Fig. 1(C) shows.

As stated above, some literatures have reported that Cu metal nanoparticles can accelerate the hydrogen production rate in highly alkaline solutions at room temperature [25,26]. They concluded that alkaline environment was necessary for their reaction. This validates the role of Cu_2O microcrystals on hydrogen generation from non-alkaline formaldehyde solution in this work. Based on this mechanism, we also can explain why the {1 1 0} surface exhibits higher activity than the {1 1 1} surface as Fig. 2(D) shows through path B in Fig. 4. Because the {1 1 0} surface has a higher number density of surface copper atoms than the {1 1 1} surface [58], the {1 1 0} surface produces more [Cu^+]·paramagnetic than the {1 1 1} surface, which is more advantageous to the generation of hydrogen from formaldehyde solution. This also explains why other semiconductor photocatalysts, such as ZnO, Bi_2O_3, Fe_2O_3, and CuO, show no activity in producing hydrogen under the same conditions. Thus, it can be seen that the formation of [Cu^+]·paramagnetic plays a vital role for hydrogen generation.

5. Conclusions

In summary, Cu_2O microcrystals demonstrate good performance in producing hydrogen and degrading formaldehyde solution under visible light irradiation. Cu_2O microcrystals play a role in two aspects of reactivity. First, the generation of electrons and holes from Cu_2O results in production of hydrogen and hydroxyl radicals. Second, the dissociation of the Cu^I—O bond of the Cu_2O microcrystal surfaces causes the formation of [Cu^+]·paramagnetic. Cu_2O with {1 1 0} surface shows higher hydrogen generation activity than Cu_2O with {1 1 1} surface. Alkaline earth oxides act as sacrifice agents to consume excessive H^+ ions and ensure retaining the activity of Cu_2O microcrystals. From the viewpoint of growing awareness of issues related to an increase in global energy demand and environment pollution, we believe that this highly efficient performance of Cu_2O microcrystals will provide a very promising method of hydrogen generation for energy supplies and formaldehyde degradation for environmental remediation.

Acknowledgments

This work was supported by the Ph.D. Programs Foundation of the Ministry of Education of China (Grant No. 20121102110027) and the National Science Foundation of China (Grant No. 51472013 and 91222110).

References

[1] C.H.B. Ng, W.Y. Fan, J. Phys. Chem. B 110 (2006) 20801–20807.
[2] C.H. Kuo, C.H. Chen, M.H. Huang, Adv. Funct. Mater. 17 (2007) 3773–3780.
[3] M. Hara, T. Kondo, M. Komoda, S. Ikeda, K. Shinohara, A. Tanaka, J.N. Kondo, K. Domen, Chem. Commun. (1998) 357–358.
[4] S. Ikeda, T. Takata, T. Kondo, G. Hitoki, M. Hara, J.N. Kondo, K. Domen, H. Hosono, H. Kawazoe, A. Tanaka, Chem. Commun. (1998) 2185–2186.
[5] M.K.I. Senevirathna, P. Pitigala, K. Tennakone, J. Photochem. Photobiol. A 171 (2005) 257–259.
[6] A.M. Mahmoud, W. Qian, M.A. El-Sayed, Nano Lett. 11 (2011) 3285–3289.
[7] W. Siripala, A. Ivanovskaya, T.F. Jaramillo, S.H. Baeck, E.W. McFarland, Sol. Energy Mater. Sol. Cells 77 (2003) 229–237.
[8] M.D. Susman, Y. Feldman, A. Vaskevich, I. Rubinstein, ACS Nano 8 (2014) 162–174.
[9] D. Nunes, A. Pimentel, P. Barquinha, P.A. Carvalho, E. Fortunato, R. Martins, J. Mater. Chem. C 2 (2014) 6097–6103.
[10] X.Y. Guo, W.Q. Lv, X.Y. Li, J. Phys. Chem. C 118 (2014) 11062–11077.
[11] Y.T. Xu, Y. Guo, C. Li, X.Y. Zhou, M.C. Tucker, X.Z. Fu, R. Sun, C.P. Wong, Nano Energy 11 (2014) 38–47.
[12] J. Chen, S.H. Shen, P.H. Guo, M. Wang, P. Wu, X.X. Wang, L.J. Guo, Appl. Catal. B-Environ. 152–153 (2014) 335–341.
[13] D.H. Jiang, W. Zhou, X.H. Zhong, Y.G. Zhang, X.H. Li, ACS Appl. Mater. Interfaces 6 (2014) 10958–10962.
[14] S.M. Majhi, P. Rai, S. Raj, B.S. Chon, K.K. Park, Y.T. Yu, ACS Appl. Mater. Interfaces 6 (2014) 7491–7497.
[15] W.X. Zhang, X.N. Yang, Q. Zhu, K. Wang, J.B. Lu, M. Chen, Z.H. Yang, Ind. Eng. Chem. Res. 53 (2014) 16316–16323.
[16] H. Jing, N. Large, Q.F. Zhang, H. Wang, J. Phys. Chem. C 118 (2014) 19948–19963.
[17] J.Y. Wang, G.B. Ji, Y.S. Liu, M.A. Gondal, X.F. Chang, Catal Commun. 46 (2014) 17–21.
[18] S.Z. Wang, B. Kavaipatti, S.J. Kim, X.Q. Pan, R. Ramesh, J.W. Agerlll, L.W. Wang, Appl. Phys. Lett. 104 (2014) 211605.
[19] Z.H. Xi, C.J. Li, L. Zhang, M.Y. Xing, J.L. Zhang, Int. J. Hydrogen Energy 39 (2014) 6345–6353.
[20] A. Martínez-García, V.K. Vendra, S. Sunkara, P. Haldankar, J. Jasinski, M.K. Sunkara, J. Mater. Chem. A 1 (2013) 15235–15241.

[21] Y.F. Zhao, Z.Y. Yang, Y.X. Zhang, L. Jing, X. Guo, Z.T. Ke, P.W. Hu, G.X. Wang, Y.M. Yan, K.N. Sun, J. Phys. Chem. C 118 (2014) 14238–14245.
[22] S. Gao, Y.F. Sun, F.C. Lei, J.W. Liu, L. Liang, T.W. Li, B.C. Pan, J.F. Zhou, Y. Xie, Nano Energy 8 (2014) 205–213.
[23] Y.X. Zhao, W.T. Wang, Y.P. Li, Y. Zhang, Z.F. Yan, Z.Y. Huo, Nanoscale 6 (2014) 195–198.
[24] Y.H. Tsai, K. Chanda, Y.T. Chu, C.Y. Chiu, M.H. Huang, Nanoscale 6 (2014) 8704–8709.
[25] D. Preti, S. Squarcialupi, G. Fachinetti, Angew. Chem. Int. Ed. 48 (2009) 4763–4766.
[26] Y.P. Bi, G.X. Lu, Int. J. Hydrogen Energy 33 (2008) 2225–2232.
[27] Y.P. Bi, G.X. Lu, Mater. Lett. 62 (2008) 2696–2699.
[28] Y.P. Bi, G.X. Lu, Chem. Commun. (2008) 6402–6404.
[29] Y.P. Bi, G.X. Lu, Nanotechnology 19 (2008) 275306–275311.
[30] Y.P. Bi, H. Hu, Q.Y. Li, G.X. Lu, Int. J. Hydrogen Energy 35 (2010) 7177–7182.
[31] H.Y. Hu, Z.B. Jiao, J.H. Ye, G.X. Lu, Y.P. Bi, Nano Energy 8 (2014) 103–109.
[32] Y. Zhang, B. Deng, T.R. Zhang, D.M. Gao, A.W. Xu, J. Phys. Chem. C 114 (2010) 5073–5079.
[33] W.Q. Zhang, L. Shi, K.B. Tang, S.M. Dou, Eur. J. Inorg. Chem. 7 (2010) 1103–1109.
[34] X.D. Liang, L. Gao, S.W. Yang, J. Sun, Adv. Mater. 21 (2009) 2068–2071.
[35] X. Lan, J.Y. Zhang, H. Gao, T.M. Wang, CrystEngComm 13 (2011) 633–636.
[36] S. Kapoor, F.A. Barnabas, M.C. Sauer, D. Meisel, C.D. Jonah, J. Phys. Chem. 99 (1995) 6857–6863.
[37] S.B. Wang, H.M. Ang, M.O. Tade, Environ. Int. 33 (2007) 694–705.
[38] T. Zubkov, D. Stahl, T.L. Thompson, D. Panayotov, O. Diwald, J.T. Yates Jr., J. Phys. Chem. B 109 (2005) 15454–15462.
[39] S. Zhang, X.S. Li, B.B. Chen, X.B. Zhu, C. Shi, A.M. Zhu, ACS Catal. 4 (2014) 3481–3489.
[40] M.J. Schilstra, G.A. Veldink, J.F.G. Vliegenthart, Biochemistry 32 (1993) 7686–7691.
[41] J.W. Yang, G.P. Shen, L.J. Wang, J.Z. Xiao, C.H. Yang, Energ. Fuel 27 (2013) 2068–2072.
[42] T. Berger, M. Sterrer, O. Diwald, E. Knoezinger, D. Panayotov, T.L. Thompson, J.T.M. Yates Jr., J. Phys. Chem. B 109 (2005) 6061–6068.
[43] Jung, A. Sharma, D. Hinderberger, S. Braun, U. Schatzschneider, E. Rentschler, Inorg. Chem. 48 (2009) 7244–7250.
[44] D.C. Hurum, A.G. Agrios, K.A. Gray, J. Phys. Chem. B 107 (2003) 4545–4549.
[45] N.M. Dimitrijevic, B.K. Vijayan, O.G. Poluektov, T. Rajh, K.A. Gray, J. Am. Chem. Soc. 133 (2011) 3964–3971.
[46] C. Jegerschold, F. MacMillan, W. Lubitz, A.W. Rutherford, Biochemistry 38 (1999) 12439–12445.
[47] H.H.T. Nguyen, K.H. Nakagawa, B. Hedman, S.J. Elliott, M.E. Lidstrom, K.O. Hodgson, S.I. Chan, J. Am. Chem. Soc. 118 (1996) 12766–12776.
[48] M. Sokmen, D.W. Allen, F. Akkas, N. Kartal, F. Acar, Water Air Soil Poll. 132 (2001) 153–163.
[49] M.N. Viswanathiah, J.A.K. Tareen, K.V. Krishnamurthy, J. Cryst. Growth 49 (1980) 189–192.
[50] S.J. Limmer, E.A. Kulp, J.A. Switzer, Langmuir 22 (2006) 10535–10539.
[51] K.G. Sun, Y.Y.V. Li, D.B.S. John, T.N. Jackson, ACS Appl. Mater. Interfaces 6 (2014) 7028–7031.
[52] M.V. Vaishampayan, I.S. Mulla, S.S. Joshi, Langmuir 27 (2011) 12751–12759.
[53] A. Goux, T. Pauport, J. Chivot, D. Lincot, Electrochim. Acta 50 (2005) 2239–2248.
[54] S.B. Wang, W.S. Yao, J.L. Lin, Z.X. Ding, X.C. Wang, Angew. Chem. Int. Ed. 53 (2014) 1034–1038.
[55] Z.Y. Zhang, B. Dong, M.Y. Zhang, J.D. Huang, F. Lin, C.L. Shao, Int. J. Hydrogen Energy 39 (2014) 19434–19443.
[56] Q.G. Dai, S.X. Bai, H. Li, W. Liu, X.Y. Wang, G.Z. Lu, Appl. Catal. B- Environ. 168 (2015) 141–155.
[57] T. Maschmeyer, M. Che, Angew. Chem. Int. Ed. 49 (2010) 1536–1539.
[58] W.C. Huang, L.M. Lyu, Y.C. Yang, M.H. Huang, J. Am. Chem. Soc. 134 (2012) 1261–1267.